Engineered Science
DOI: https://dx.doi.org/10.30919/es1028

The Behavior of Thermal Shock Repairing of High Strength Reinforced Concrete Beam Using NSM-CFRP Rope and Strip

Ahmed M. Ashteyat,[1] Ala' Taleb Obaidat[2,*] and Tarik Fayez Kharabsheh[1]

Abstract

Experimental research was performed on the flexural strength capacity of RC beams subjected to thermal shock after heated to 500 °C and 700 °C for three hours, and then quickly cooled using a CO_2 fire extinguisher or water immersion. Different near Surface Mounted (NSM) including rope and strip were used to repair the damaged beams. A four-point flexural test specimen's response is recorded. The results demonstrated that, depending on the heat-shock treatment, both compressive and tensile strength decreased significantly (66-42% and 74-30%, respectively) of the control specimens. The flexural capacity of high-strength RC beams decreased to 88.2–95.1% of the control specimens after being subjected to different cooling regimes. However, when CFRP ropes and strips were used for repair, the flexural capacity of each specimen was restored to a minimum of 107% and a maximum of 177% of their original flexural capacity. Among the repair configurations, the side trapezoidal profile and bottom NSM were found to be the most effective. The failure modes shifted from flexural failure in the control specimens to shear or a combination of shear and CFRP rupture failure in specimens repaired using CFRP, except for those repaired with straight-line side NSM.

Keywords: Carbon fibre reinforced polymers; Thermal shock; CO_2 fire; Water-cooled; Flexural behavior.
Received: 26 September 2023; Revised: 08 November 2023; Accepted: 08 November 2023.
Article type: Research article.

1. Introduction

The effects of fire on Reinforced Concrete (RC) structural elements and, in more severe situations, the thermal shock caused by firefighters using CO_2 or water to extinguish the flames, which results in significant cracks, are two evident issues. Due to the invention of current additives like superplasticizers, high strength concrete (HSC) has come to be widely recognized in the industry due to its lower cost-per-strength ratio and more economically viable than Normal Strength Concrete (NSC).[1-3] The effects of heat load on concrete have been extensively studied; exposure to high thermal loads has a negative impact on concrete's compressive strength, elastic modulus, and stress-strain relationship.[4-7] Neville[7] examined how fire affected (NSC) and found that at temperatures of 300 °C or higher, mechanical properties all shown loss due to heat stress, according to a comparative investigation by Ma *et al*..[8]

Researchers discovered that quick cooling following exposure to high temperatures causes structural elements to experience a thermal shock, which causes significant microcracks and a loss in mechanical characteristics.[9,10] The sort of cooling technique, such as submersion in water, water spraying, or the use of CO2, also affects the result. Depending on the cooling technique, water-cooled specimens have an extra strength decrease of up to 38% compared to slowly cooled specimens.[11] When the concrete is subjected to higher temperatures, the difference between the cooling processes, however, decreases. This is because concrete and the reinforcing have a strong bond but are extremely sensitive to high temperatures and subsequent cooling.[12] After the specimens were heated at 700 °C, Bingöl, and Gül,[13] utilized fast cooling in water and air. The findings indicated that water-cooled specimens had significant strength loss. According to Al- Rousan *et al*.,[14] the thermal shock significantly affects the mechanical and structural performance of the beam by reducing its shear capacity and stiffness and, as a result, causing the concrete to crack extensively without spalling.

There have been several experimental research on the fire performance of NSC beams, and to a lesser extent on HSC beams, according to a thorough assessment of the literature. Odeyemi *et al*,[15] examined the mechanical properties of HPC

[1] *Civil Engineering Department, the University of Jordan, Amman 11942, Jordan.*
[2] *Civil Engineering Department, Philadelphia University, Amman 19392, Jordan.*
**Email:* aobaidat@philadelphia.edu.jo, atobaidat@gmail.com (A. Obaidat)

supplemented with Guinea Corn Husk Ash (GCHA) in place of cement. Abdulrahman and Abdul Kadir[2] investigated the flexural behavior of fire-damaged HSC beams over a variety of fire exposure durations before reinforcing them with CFRP. According to the test findings, all specimens failed in a flexural manner with only moderate spalling. While the deflection at failure was almost identical to the control beam. The capacity increased by 34% above the control beam after strengthening, and the effect of fire was significantly reduced. To compare the performance of high and NSC in fire situations, Ali[16] evaluated 18 concrete columns. The findings showed that, under loading alone, that is, without axial constraint, both NSC and HSC columns exhibited a similar sensitivity to explosive spalling. When tested while restrained, NSC columns had increased spalling degrees. Choi and shin[17] examined the impact of concrete compressive strength and cover thickness on the RC beams' structural performance under fire. The results revealed that before spalling, the rates of deflection increased similarly for concrete beams with normal strength and those with high strength, but they dramatically increased for those with high strength after spalling. For NSC beams, the cover thickness affected the failure time, but not for HSC beams. According to,[18-20] spalling caused HSC columns to have more severe fire resistance than standard strength concrete NSC columns.

In order to prevent structural capacity loss and repair RC members to recover the loss of mechanical performance, researchers are looking for new materials and methodologies such as Fiber Reinforced Polymers (FRP). High tensile strength, corrosion resistance, and simple installation, and reduced installation and maintenance costs are a few of the advantages of using FRP.[21-34] The NSM technique is commonly used for strengthening RC structural elements. NSM method involves embedding FRP into prepared grooves in the concrete.[35-38]

NSM-CFRP rope or strip has been used by a number of researchers to reinforce or repair structures that have been damaged by heat or preloading.[29,33,39-42] It was discovered that NSM-CFRP rope is extremely effective for improving the performance of damaged beams. Sharaky *et al.* 2014[43] revealed that the concrete beams strengthened by NSM Glass FRP and Carbon FRP exhibited an increase in ultimate strength of around 159% and 166%, respectively when compared to equivalent non-strengthened specimens. Sharaky *et al*. 2017[44] examined the behavior of reinforced concrete beams (RC beams) with and without end anchoring using numerical and experimental methods. Experimental research on the mechanical performance of post-heated reinforced concrete beams is conducted by Haddad and Harb[45] utilizing NSM-CFRP rope. The results indicated that rehabilitated beams lost just a little amount of their rotational ductility while recovering some or all of their original load capacity. Cantilever self-Compacting concrete (SCC) beams were researched by Ashteyat *et al*.[46] employing Side Near Surface mounted (SNSM) FRP for strengthening or repairing. The number and location of SNSM CFRP strips, as well as the exposure temperature, were shown to have a substantial influence on the mechanical performance of the current SCC cantilever beam. Additionally, when heat-induced damage increases, the advantage of restoration utilizing various SNSM CFRP strip methods increases. The behavior of self-compacted cantilever concrete SCCC beams subjected to high temperatures and repaired using NSM-CFRP rope was examined by Obaidat *et al*..[33] The results demonstrated that, in comparison to other techniques, the use of NSM-CFRP rope as retrofitting or strengthening procedures along the sides of cantilever beam had a substantial impact on load-deflection behavior. Two CFRP ropes at the sides and top surface of repaired SCC beam specimens that had been damaged by heat up to 500 °C for two hours showed similar load capacities to control specimens of around 197% and 101%, respectively.

Many of the buildings built by HSC are subjected to high temperatures, which may severely damage them. This is especially true when thermal shock occurs, such as quick cooling, which can result in substantial microcracks and a loss of mechanical properties. Therefore, research on the behavior of HSC beams subjected to thermal shock after exposure to high temperatures is essential. In recent years, there has been a substantial increase in study into the use of FRP in repairing and rehabilitating RC structures; the majority of this research has focused on NSM systems employing CFRP strips or rods. However, Studies on the usage of CFRP ropes are scarcer. Although it is expected that using CFRP-ropes and strips will help any heat-damaged structural an element recover its capacity. The effectiveness of using CFRP ropes to repair HSC beams damaged by high temperatures has not been thoroughly investigated. Moreover, there is a lack of thorough research on the behavior of HSC beams exposed to thermal shock, which includes CO_2 and water. The main objective of this research is to assess how thermal shock, which includes CO_2 and water, influences how HSC beams behave after being exposed to high temperatures. Additionally, employing NSM-CFRP strips and ropes, innovative repair methods for thermally shocked flexural deficient beams will be proposed.

2. Experimental program

2.1 Materials

2.1.1 Concrete and steel reinforcement

All of the beam specimens and additional testing cylinders were cast using Ready-mix HSC. The concrete mix design provided by a commercial ready-mix supplier is shown in Table 1. Other than superplasticizers, no other special additives were employed in the mixture besides ordinary Portland Cement (OPC) to achieve the observed strength. According to the manufacturer's instructions, all of the specimens and cylinders were cast simultaneously and as quickly as feasible (within two hours). The test beams and cylinders were cured for 28 days in accordance with the ACI Code. To determine the concrete's compressive strength, three concrete cylinders measuring 300 mm in height and 150 mm

in diameter were placed to the test. The identical concrete mix was used to construct each tested specimen of RC beams. In order to achieve a 28-day compressive cylinder strength of 60 MPa, a concrete mixture was created in accordance with the ACI-211 mix design technique (American Concrete Institute, 1996).

Table 1. Mix design proportions.

Materials for Proportioning	Volume (L/m³)	Oven-dry Weight (kg/m³)
Cement OPC	142.9	450.0
Water	139.5 (Free water)	171.3 (Total water)
Coarse Aggregate	117.5	299.6
Medium Aggregate	207.3	527.5
Fine Aggregate I	103.6	264.6
Fine Aggregate (Silica Sand)	262.5	681.9
Admixture (Adcon PC550)	6.8	8.0
Air Voids	20.0	n/a
Total	1,000.0	2,402.9 [3,4]

Deformed 12 and 10 grade 60 bars were employed for flexural reinforcement, and 8 mm smooth stirrups were used for shear. In Section 2.2.1, the design process for the beams is described in extensive detail.

2.1.2 CFRP and adhesives

For specimen strengthening, commercially available CFRP ropes (SikaWrap FX-50C) and CFRP strips (Sika) were combined with (SikaDur 52) saturating resin. As for the adhesive, it was utilized in two parts, combined in accordance with the manufacturer's instructions (SikaDur 330). The commercial provider (Sika AG) provided all the CFRP and adhesive materials in Fig. 1.

Fig. 1 SikaWrap FX 50C CFRP ropes.

Table 2 specifies the geometric and mechanical properties of CFRP Ropes and Strips. While Tables 3 and Table 4 define the properties of the resins and adhesives as supplied by the manufacturer.

Table 2. Sika Wrap FX 50C properties.

Construction	Unidirectional carbon fibre string encased in a plastic envelope	
Fibre Type	Carbon fibre	
Packaging	25 m roll on a plastic reel dispenser	
Shelf life	24 months from the date of production	
Storage conditions	Store in undamaged, original sealed packaging in dry conditions at temperatures between +5 °C and +35 °C. Protect from direct sunlight.	
Dry Fibre Density	1.82 g/cm³	
Cross Section	≥ 28 mm² (based on carbon fibre content)	
Mass per Unit Length	≥ 50 g/m (based on carbon fibre content)	
Dry Fibre Tensile Strength	4 000 N/mm²	(ASTM D 4018)
Dry Fibre Modulus of Elasticity in Tension	240 kN/mm²	(ASTM D 4018)
Dry Fibre Elongation at Break	≥ 1.6%	(ASTM D 4018)
Laminate Nominal Cross Section	78 mm²	
Laminate Tensile Strength	~2 000 N/mm² (related to fibre cross-section)* *Impregnating resin: Sikadur®-300 or Sikadur8-52 LP **Values in the longitudinal direction of the fibres ***Standard adapted to fit sample shape	(EN 2561**)
Laminate Modulus of Elasticity in Tension	~230 kN/mm² (related to fibre cross-section)* *Impregnating resin: Sikadur*-300 or Sikadur®-52 L **Values in the longitudinal direction of the fibres ***Standard adapted to fit sample shape	(EN 2561**)

2.2 Beam specimens

2.2.1 Beam design

According to ACI 318-19,[47] To avoid shear failure, fifteen rectangular beams were designed with higher shear capacity. As illustrated in Fig. 2, all specimens were reinforced with two 10 mm diameter bars as top reinforcement, two 12 mm diameter bars as bottom reinforcement, and 8 mm stirrups bars placed at 100 mm as transverse reinforcement. For the

Table 3. SikaDur 52LP properties.

Compressive Strength	>70 N/mm² (7 d / 30 °C)	(ASTM D695)
Tensile Strength	~27 N/mm² (7 d / 30 °C)	(ISO 527)
Tensile Adhesion Strength	Curing time: Curing temperature 25 °C 2 days: >7 N/mm² 14 days: >10 N/mm²	
Density	Part A+B mixed (2:1)	+20 °C ~1.06 kg/l

Table 4. SikaDur 330 properties.

Modulus of Elasticity in Flexure	~3800 N/mm2(7 d, +23 °C)			(DIN EN 1465)
Tensile Strength	~30 N/mm² ((7 d, +23°C)			(ISO 527)
Modulus of Elasticity in Tension	~4500 N/mm2(7 d, +23 °C)			(ISO 527)
Elongation at Break	~0.9 % (7 d, +23 °C)			(ISO 527)
Tensile Adhesion Strength	Concrete fracture (> 4 N/mm²) on a sandblasted substrate			(EN ISO 4624)
Coefficient of Thermal Expansion	4.5 x 10^{-5} 1/K (Temperature range -10 °C min. / +40 °C max.)			(EN 1770)
Glass Transition Temperature	Curing time: 30 d	Curing temperature: +30°	TG: +58 °C	(EN 12614)
Heat Deflection Temperature	Curing time: 7 d 7 d 7 d	Curing temperature: +10 °C +23 °C +35 °C	HDT: +36 °C +47 °C +53 °C	(ASTM D 648)
Service Temperature	Resistance to continuous exposure up to +45 °C -40 °C min. / +45 °C max.			

longitudinal steel bars, the corresponding values were 420 MPa for yield strength, 562 MPa for ultimate strength, and 10% for elongation at failure. Whereas the average yield strength of the shear reinforcement steel was about 370 MPa, 470 MPa for ultimate strength with 3.8% elongation. To determine the mechanical characteristics of steel bars, a tensile test was performed at room temperature on all diameters (Table 5).

2.2.2 Beam construction

18 mm fair-faced plywood was used to create wooden formwork casts that were 150 x 250 x 1400 mm in size. As seen in Fig. 3, the formwork molds were securely attached to guarantee that the beams maintained their proportions throughout the casting process. For an equal finish, the molds were also set on a level, spotless sand surface. To guarantee a stable geometry of the beams, the steel cages were then put into the molds, the spacers were precisely adjusted, and the wood molds were secured and set on a level sandy surface. All seventeen molds were cast with commercially available ready-mix HSC, and an electric concrete vibrator was used for compacting the mixture (see Fig. 4). When the casting of the beams was finished, surface polishing was carried out. Thirty test cylinders were made from the ready-mix concrete at the same time. As illustrated in Fig. 4, the beams and cylinders were wrapped in burlap after the concrete casting process was finished to stop moisture loss and shrinkage. The beams and the cylinders' formwork was taken off the next day.

2.3 Test matrix

This research was divided into two heat-shock treatments, seven repairing configurations, and two CFRP types. The investigation's test matrix, grooving configuration profiles, and other testing parameters are all included in this section. The specimens are distributed as shown in Fig. 5 and Table 6. The grooves were cut using an electrical drill with dimensions of 25 mm for depth and 15 mm (8 mm for strips) for width, as shown in Fig. 6. Six configurations were tested strengthening

Table 5. Mechanical properties of the reinforcing steel bars.

Nominal Bar Diameter	Actual Bar diameter	Yield Stress fy (MPa)	Ultimate Stress, fu (MPa)	Elongation at Failure (%)
10 mm	10.3	420	562	10
8 mm	8.1	370	470	3.8
12mm	12.3	420	562	10

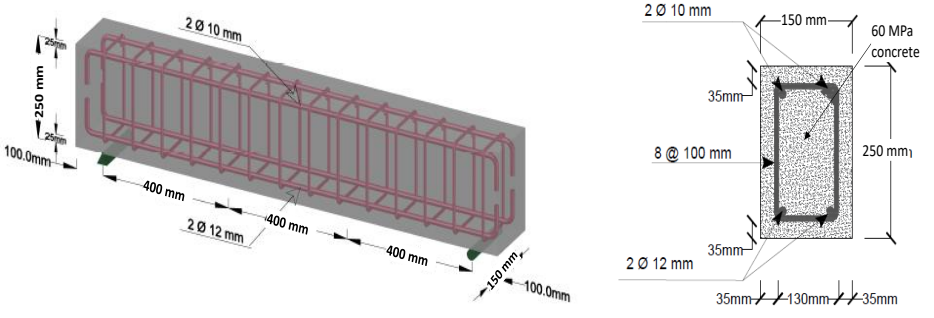

Fig. 2 Beam design profile and cross-section.

Fig. 3 Casting molds fastened and prepared for concrete casting on a sand surface.

Table 6. Temperature and cooling method treatments.

Beam Designation	Treatment		Tested variable
	Temperature °C	Cooling	
25-N-0	25	None	-
25-N-0	25	None	-
700-C-0	700	CO2	Effect of Configuration on CO_2 cooling
700-C-1	700	CO2	
700-W-0	700	Water	Effect of Configuration on water cooling
700-W-1	700	Water	
700-W-2	700	Water	
700-W-3	700	Water	
700-W-4	700	Water	
700-W-5	700	Water	
700-W-6	700	Water	
700-W-7	700	Water	
500-W-0	500	Water	Effect of type of cooling
500-W-1	500	Water	
500-C-1	500	CO2	

with CFRP rope, and one configuration using CFRP strips. The first configuration had two main longitudinal grooves cut into the bottom side of the beam, measuring 1400 mm in length; the second configuration had the same two straight grooves, but on the sides of the beam. Configurations 3 & 4 used trapezoidal and parabolic grooves to more closely follow the moment profile. Then, configurations 5 & 6 were tested to examine the effect of using localized bottom CFRP in the high-tension zone (middle of span). Finally, a different repairing material (CFRP strips) was used in Configuration 7, which had two bottom grooves 25 mm deep and 8 mm wide.

Every specimen has a distinctive designation, where the letters W, C, and N stand for water, CO2, and non-cooling, respectively. For example, in specimen 700-C-1, number one indicates the CFRP configuration one, number C indicates the CO2, and the first number indicates the temperature in degrees. The configuration profiles are illustrated in Figs. 5 and 6, detailing the geometry of the grooving and the types of CFRP used (Strips or Ropes).

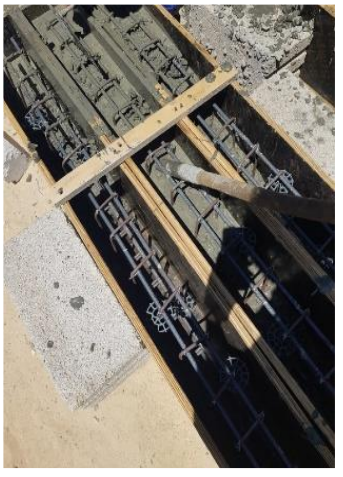

Electric concrete vibrator

Beams covered in burlap for curing

Fig. 4 casting and curing process.

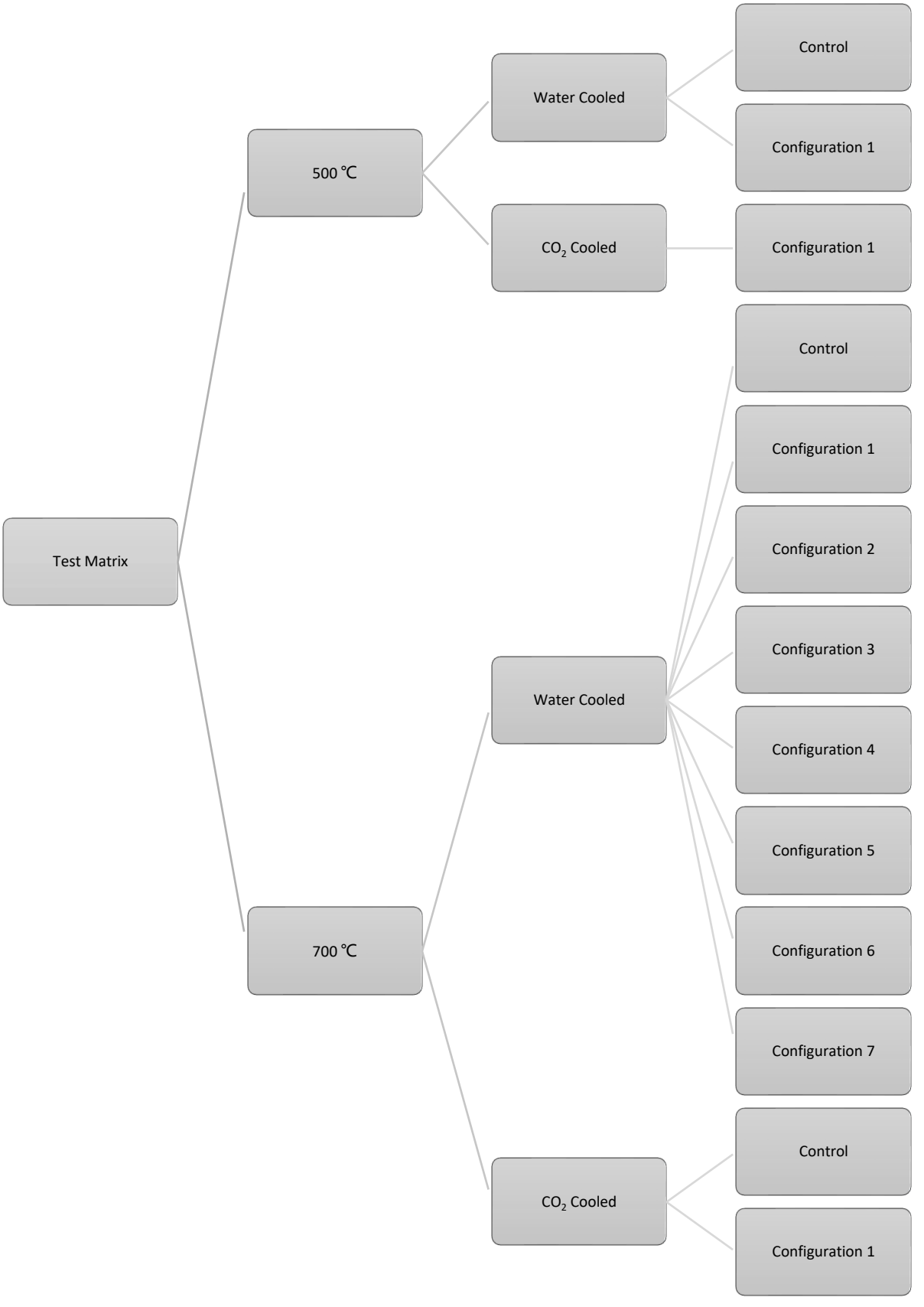

Fig. 5 Test matrix.

Configuration	CFRP Groove (mm)	Notes
0	None	Control
1	Bottom 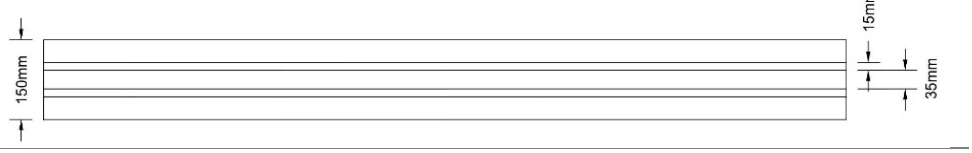 Side None	CFRP ropes
2	Bottom None 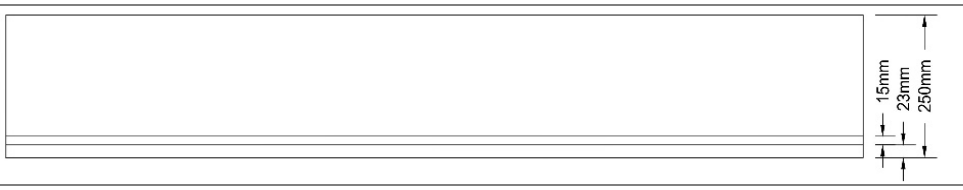 Side	CFRP ropes
3	Bottom None 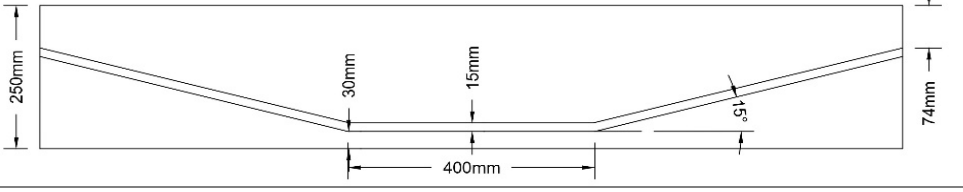 Side	CFRP ropes
4	Bottom None 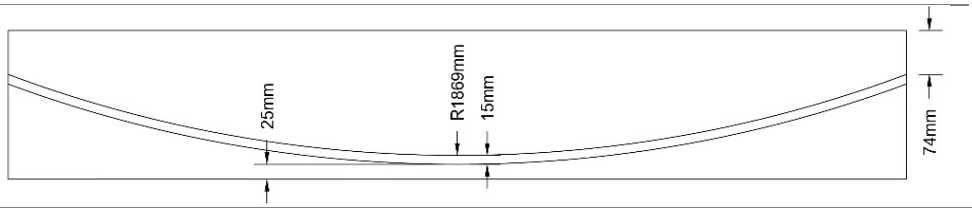 Side	CFRP ropes
5	Bottom 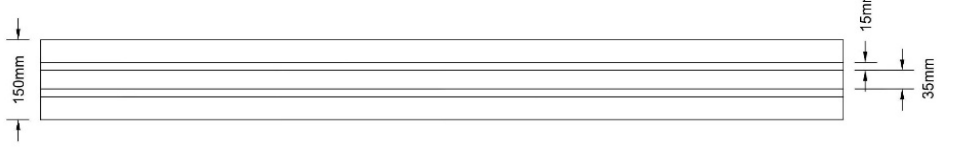	CFRP ropes

Fig. 6 Configuration profiles and materials.

2.4 Thermal shock process

The specimens were heated in an electrical furnace with internal measurements of 2 × 1.5 × 1 m (Fig. 7). The furnace has temperature sensors and a control module to adjust the times and temperatures, and its maximum power is 24 kW. Based on temperature, RC beams have been divided into three groups for this experimental study. The temperature of the first category was normal, the second category was exposed to 500 °C., and the third category was subjected to 700 °C. After the RC beams were placed into the furnace, the temperature was raised to the desired level. Beam specimens remained at the required temperature for three hours. In Fig. 8, the rate of heating is displayed.

Fig. 7 Testing electric furnace.

The furnace lid is safely opened after the heating cycle is complete. As seen in Fig. 9, the beams are transported by the crane one at a time to be quickly cooled either by immersion in a ready water tank nearby or by a CO_2 extinguisher. Since this procedure is dangerous, safety measures were implemented while emergency professionals were present in the lab. The cracks produced on by the heat shock are markedly visible when the beams have cooled to ambient temperature. The specimen then undergoes the CFRP application and grooving processes.

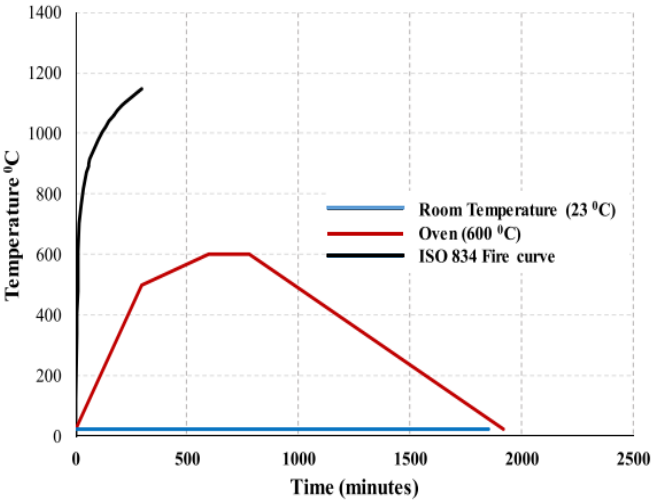

Fig. 8 Heating rate.

2.5 Grooving and FRP installation

In order to increase the specimen's capacity for tension, the NSM approach requires the application of CFRP reinforcement. In this part, the steps for groove preparation, cutting, applying CFRP and adhesive, and curing are described in detail.

2.5.1 Grooving and surface preparation

To make the edges of the grooves more visible, the beams were painted an obvious white. The beam was correctly oriented before the groove outlines were precisely drawn on the beam in accordance with the schematics, as illustrated in Fig. 10. As illustrated in Fig. 10. The grooves and anchors were cut with an electric rotary saw blade, chipped with a hammer, and cleaned. The mid-span cross-section detailing grooves for 'Configuration 1' are shown in Fig. 11 and have dimensions of 8 mm wide and 25 mm deep for the strips and 15 mm wide and 25 mm deep for the ropes.

Fig. 9 Placement of specimens into water and Cooling of specimens using a CO_2 fire extinguisher.

Fig. 10 Outlining the grooving perimeters and Grooving using a rotary saw blade.

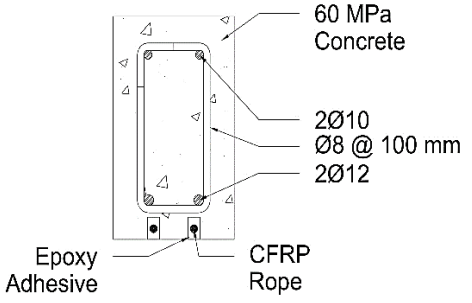

Fig. 11 Cross-section at mid-span for Configuration1.

2.5.2 CFRP application and curing

The length-appropriate ropes and strips of CFRP were cut. Using the saturating glue provided by the manufacturer, the CFRP rope was soaked. Then, two-part epoxy was properly mixed in accordance with the manufacturer's specifications (Sikadur 330 for ropes and Sikadur 30 for strips). To prevent air gaps, the groove was partially filled before CFRP was inserted, and the remaining space was filled and removed. This procedure is seen in Fig. 12. The epoxy adhesive was next allowed to cure for seven days at room temperature in accordance with the manufacturer's recommendations before moving on to the testing stage.

Fig. 12 Grooves filled with epoxy adhesive.

2.5.3 Test Setup At the University of Jordan's Structures Lab, the specimens were placed to the test using a 4-Point static load hydraulic jack to determine their flexural capacity and response. To measure the linear displacement of the specimens under load, two LVDTs were mounted on the beam mid-span and two more at each one-third point of the span; the LVDT is connected to a data gathering device. The test setup and control devices are shown in Fig. 13. Using Load control, the load increased gradually at a constant rate of 3 kN/sec. A data acquisition system was used to capture the test results.

Fig. 13 Flexural test setup.

3. Test results and discussion

3.1 Mechanical properties

Thirty concrete cylinders were examined; fifteen were used for compressive tests and fifteen were used for splitting tensile tests. Three test specimens were used for each concrete treatment (different heating temperature and cooling procedure). The findings of mechanical properties for all specimens are listed in Table 7. These HSC specimens were exposed to temperatures as high as 500 °C and 700 °C for three hours before being quickly cooled with water and a CO_2 fire extinguisher. The residual compressive and tensile stress capacity was significantly impacted by these treatments as seen Table 6, Figs. 14 and 15.

Table 7. Test results of mechanical properties.

Specimen treatment	Compressive test (MPa)	Tensile splitting test (MPa)
Unheated control	55.2	3.74
Heated to 500 °C, water-cooled	23.40	1.67
Heated to 500 °C, CO_2 cooled	31.90	2.60
Heated to 700 °C, water-cooled	22.8	1.51
Heated to 700 °C, CO_2 cooled	18.90	0.97

The decreased Ca (OH)2 concentration and the un-hydrated area function are the main contributors to this

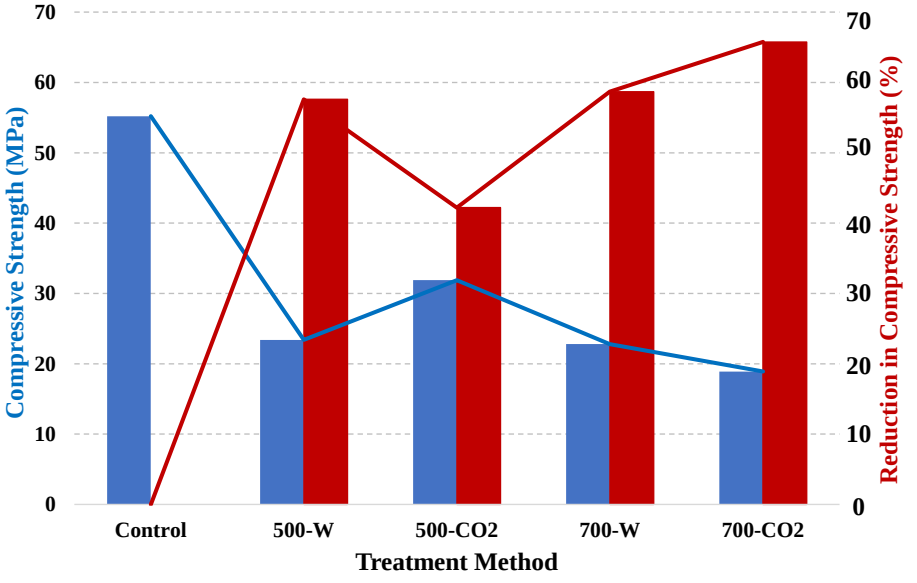

Fig. 14 Compressive stress results.

strength loss at high temperatures.[9] At 700 °C compared to 500 °C, the drop in compressive and tensile stress was more pronounced. A higher temperature above 150 °C will result in a decrease in concrete's compressive and tensile strength due of the loss of free absorbed water and the decomposition of Ca (OH)2.[57,58] This finding is supported by other investigations.[9] However, the cooling technique had a temperature-dependent impact; as shown in Fig. 14, water cooling resulted in a more notable loss of strength than CO_2 fire extinguisher at 500 °C than it did at 700 °C. Regardless of the heating temperature, water cooling reduced compressive stress to almost the same level (58% capacity decrease at 500 °C and 59% at 700 °C). According to,[11] typical concrete's compressive strength decreased by 28% to 35%. The decrease for water cooling beyond 500C was shown in[13] to be 30%. Temperature had a minor impact on tensile strength loss, with a 55% decrease at 500 °C and a 60% retention at 700 °C. Cooling by CO_2 decreased the compressive strength 42% at 500 °C, 66% at 700 °C. The tensile data showed the same trend, with CO_2 cooling leading to a greater loss of tensile strength at 700 °C (74% decrease) than at 500 °C (30% decrease), Fig. 15. The more substantial effect was generated by the more extreme temperature differential between 700 °C and the CO_2 temperature at the extinguisher's nozzle, which was -66 °C. Overall, it can be concluded that all heat shock treatments resulted in a loss of compressive and tensile strength, although CO_2 produced a more severe loss at the higher temperature (700 °C), and water-cooled specimens produced a similar loss of strength regardless of temperature.

3.2 Crack pattern

The heat shock cracks were mapped after the beams were cooled to room temperature. Spider web thermal cracks, as seen in Fig. 16, developed at both elevated temperatures due to the quick loss of water content in concrete and the expansion of the concrete under thermal strain. According to

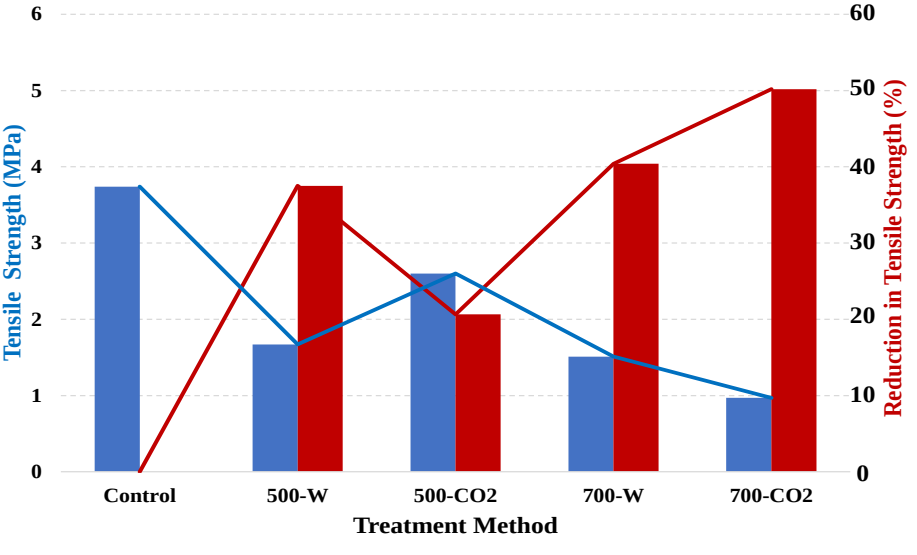

Fig. 15 Tensile stress results.

Fig. 16, cooling by water immersion generated highly dense and narrow cracks, whereas cooling by CO_2 fire extinguisher produced less dense but wider cracks. The cooling technique had an impact on the density and form of the spider web thermal cracks in the concrete.

Fig. 16 Spider web cracks caused by heat-shock.

3.3 Flexural Tests Results

Table 8 summarizes the test findings for each beam specimen, including yield load, yield displacement, ultimate load, ultimate displacement, percentage of control specimen, first cracking load, and failure mode.

3.3.1 Effect of heating temperature (500 °C vs 700 °C)

Two control specimens (500-W-0 and 700-W-0) were cast and heated to 500 °C and 700 °C, respectively. Fig. 17 illustrates the load-deflection relationship, which begins linearly up to the yield point, tapers as it approaches the ultimate load, then steadies before ductile failure. The ultimate flexural capacity of the heat-damaged beams did not considerably decrease in comparison to the control, according to test results on specimens 500-W-0 and 700-W-0. As seen in Fig. 18, a number of test specimens exhibited explosive spalling during heating. This was caused by the vapor pressure inside the specimen building up and the quick heating process not giving the pressure the time to release via the microcracks in the concrete.[48,49]

The water content in the remaining specimens that did not explode spall were heated at a slower rate, which maintained it below the essential water content established by Harmathy. The ultimate capacity of the control specimens was 163.9 kN, but the capacities of the specimens 500-W-0 and 700-W-0 were 153.68 kN and 152.17 kN, respectively. The higher temperature (500 °C or 700 °C) cannot be inferred to have a significant impact on the ultimate flexural capacity of HSC beams intended to fail in flexure. While the final deflection increased by 6% and 16% correspondingly at 500 °C and 700 °C. The first cracks in control unheated beams appeared at 47 kN, the first cracks for the specimen heated to 500 °C appeared at 60 kN, and the first cracks for the specimen heated to 700 °C appeared at 110 kN. This result indicates that the higher temperature treatment made the flexural beam more brittle, or that the concrete outer layers became less suitable for flexural cracks. The heated specimens' yielding loads, which were 130 kN for the control, dropped to 123 kN at 500 °C and 112 kN at 700 °C.

3.3.2 Effect of cooling method (Water vs CO_2)

How the cooling technique will impact the properties of the examined specimens is a further comparison that should be

Table 8. Experimental results of Flexural test.

Beam	Ultimate Load		Ultimate Displacement		Yield Load	Yield Displacement	First crack (kN)	Failure[1]
	UL (kN)	% UL	Us (mm)	%Ud	YL (kN)	Yd (mm)		
25-N-0-1	159.36	-	73.61	-	142	26.94	47	FF
25-N-0-2	163.85	-	27.89	-	130	10.69	57	FF
700-W-0	152.17	94.2	32.46	116.4	112	5.92	110	FF
700-W-1	259.34	160.5	23.36	83.8	146	8.08	120	SF, FR
700-W-2	212.7	131.6	20.15	72.2	129	6.95	110	FD, CS
700-W-3	276.65	171.2	24.9	89.3	149	6.28	130	SF, FR
700-W-4	255.56	158.1	27.27	97.8	130	6.46	130	SF, FR
700-W-5	283.17	175.2	20.34	72.9	181	9.85	140	SF, FR
700-W-6	279.84	173.2	23.5	84.3	165	6.75	150	FR, CS
700-W-7	250.24	154.8	23.58	84.5	138	6.73	130	SF
700-C-0	149.5	92.5	27.86	99.9	108	8.17	80	FF
700-C-1	172.56	106.8	17.13	61.4	145	10.96	90	SF, FR
500-W-0	153.68	95.1	29.5	105.8	123	8.38	60	FF
500-W-1	263.64	163.1	24.39	87.5	187	11.28	90	FF, SF, CS
500-C-1	285.87	176.9	26.01	93.3	201	13.92	60	SF, FR

UL: Ultimate Load; Us: Ultimate Displacement; YL: Yield Load; Yd: Yield Displacement

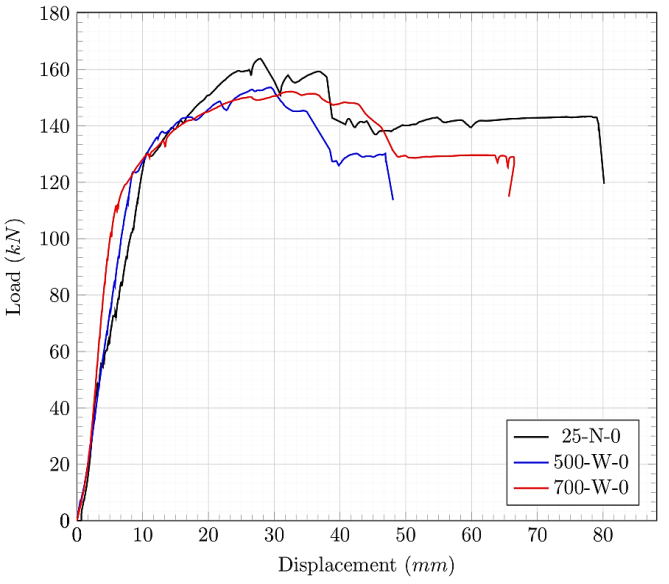

Fig. 17 Effect of the heating temperature load-deflection curve.

Fig. 18 Explosive spalling of beam specimens.

made. The curve begins as a straight line up to the yield point, tapers, approaches maximum load, then steadies before ductile failure, as seen in the load-deflection diagram (Fig. 19). Results from the testing of specimens 25-N-0, 700-W-0, and 700-C-0 indicate that the ultimate flexural capacity of the heat-damaged beams behaved differently based on the cooling method used. The control specimens had an average strength of 161.1 kN, however the specimens 700-W-0 and 700-C-0 had maximum capacities of 152.7 kN and 149.5 kN, respectively. Therefore, it cannot be said that the final flexural capacity of HSC beams intended to fail in flexure was unaffected by the cooling method used to cool HSC beams (water or CO_2). As can be observed, thermal shock caused by water increased the final deflection by around 16%.

3.3.3 Effect of repair configuration (Bottom vs Side NSM)

The load displacement for specimens repaired with NSM-CFRP is shown in Fig. 20. The Fig. 20 shows how the loading develops linearly until the failure point before failing suddenly as a result of shear failure and FRP debonding. As can be observed, the final capacity is improved when RC beams are repaired utilizing any form of arrangement. A Side NSM can reach larger capacities, but it relies on the strengthening profile, according to the findings of testing specimens repaired using CFRP rope at the bottom and sides of the beam.[45]

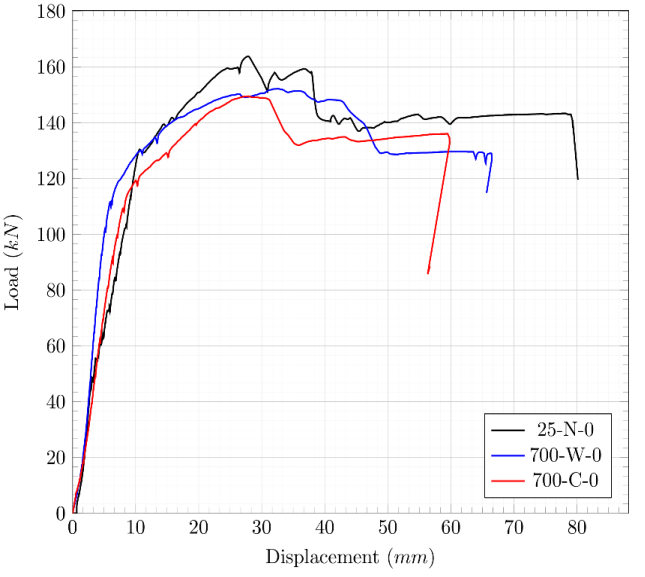

Fig. 19 Effect of the cooling method load-deflection curve.

The maximal load for the restored bottom-face beams was 259.3 kN, which is [160%] more than the heated control's 152.2 kN. At 276.7 kN (182% more than control), the beams repaired with Side NSM in a trapezoidal shape (700-W-3) performed better than the others. However, the ultimate load is reduced to 212.7 kN (140% less than control) when strengthening with a straight profile (700-W-2). indicating that Bottom NSM has only one possible configuration: straight lines, and that Side NSM will provide better results based on the configuration. The rapid shear failure that occurred caused a considerable reduction in the final capacity for repaired specimens between 17% and 28% compared to control specimens, as shown in Fig. 20. First cracks and crack patterns were similar; for 700-W-2, 700-W-1, and 700-W-3, first cracks developed at 110 kN, 120 kN, and 130 kN, respectively. As can be observed, as compared to the control sample, the repaired RC utilizing FRP greatly delays the onset of the first cracking

3.3.4 Effect of repair configuration (Economic use of Bottom NSM CFRP)

This section compares the beam 700-W-5, which combines two full-length Bottom NSM ropes with a trapezoidal Side NSM, with the beam 700-W-6, which has an identical layout but only uses half-length Bottom NSM ropes. The load-deflection diagram in Fig. 21 starts linearly and continues until it reaches the point of failure, when the beam collapses suddenly and without a ductile reaction. Because the half-length FRP ropes were positioned in the middle span tension

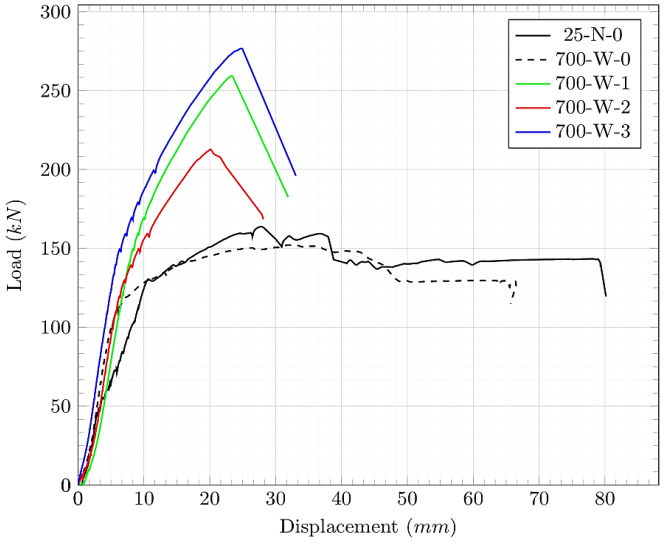

Fig. 20 Effect of NSM location load-deflection curve.

zone, the results reveal that using less FRP material had no noticeable effect on the ultimate load capacity. This indicates that halving the number of FRP ropes used in the bottom face only slightly decreased the ultimate flexural load by 3.4 kN (1% difference), as the specimen repaired with two side ropes and two full-length ones (700-W-5) reached an ultimate load of 283.2 kN (186% of the control specimen), and the specimen with two side ropes and two half-length ones (700-W-6) reached an ultimate load of 279.8 kN (184% of the control). However, compared to the control beam, the deflection decreased by 28% and 22% and the elastic stiffness increased by 140% and 130% for 700-W-5 and 700-W-6 respectively.

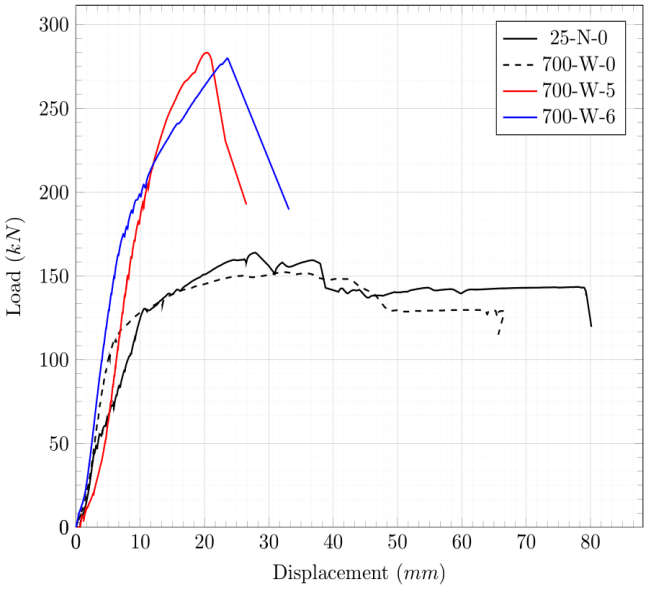

Fig. 21 Effect of economic use of CFRP rope load-deflection curve.

The first cracks and cracking behavior were similar for the two configurations; 700-W-5 (full-length) experienced a combined shear failure and FRP rupture at 140 kN, while 700-W-6 (half-length) experienced a flexural-shear failure combined with FRP rupture and concrete cover separation of the bottom face at 150 kN. The sudden collapse of the specimens was unaffected by the introduction of half-length ropes at the bottom.

3.3.5 Effect of repair configuration (Side NSM Trapezoidal vs Parabolic)

Minor differences in behavior can be observed when comparing the trapezoidal Side NSM (700-W-3) and parabolic Side NSM (700-W-4) profiles in terms of failure mode, first cracking, and ultimate loads. The specimen 700-W-3 with a trapezoidal profile achieved a slightly higher ultimate load at 276.65 kN compared to 700-W-4 with a parabolic profile at 255.56 kN, representing an 8% increase (Fig. 22). Although this increase was modest, it is worth noting that the amount of FRP used for both beams was nearly identical. This suggests that the use of a trapezoidal Side NSM profile may be more advantageous in terms of ultimate capacity.

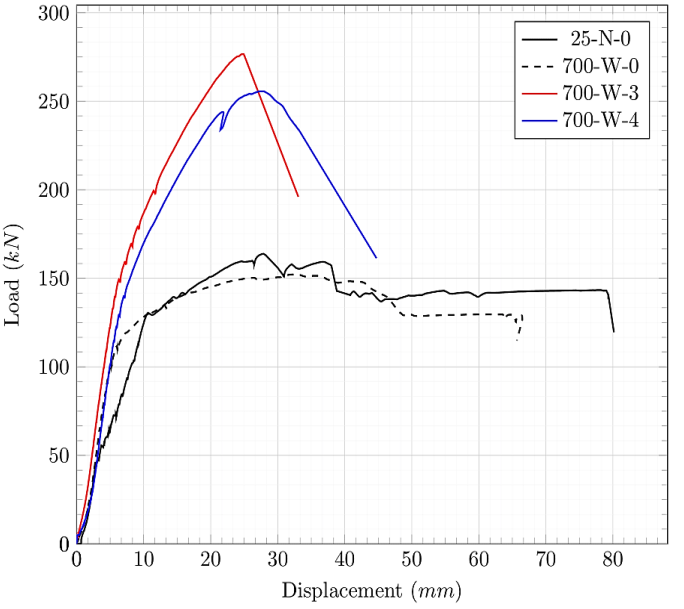

Fig. 22 Effect of side NSM profile load-deflection curve.

The shear failure and FRP rupture failure modes were combined in both failures, and the cracking behavior and initial cracks were identical for the two configurations (Figs. 24g & h). Both materials attained the first cracking load at 130 kN. The load-deflection curve illustrated in Fig. 22, which begins with a linear region and ends at the ultimate load point, clearly shows that this rupture and concrete shear caused a sudden failure.

3.3.6 Effect of CFRP material (Rope vs Strip)

The test results for specimens 700-W-1 (ropes) and 700-W-7 (strips) demonstrate a significant increase in the ultimate flexural capacity of the heat-damaged beams when repaired using CFRP ropes and strips, as compared to the control. The beam repaired using CFRP rope increased its flexural capacity

to 259.3 kN. This represents a substantial recovery of the heat-damaged beam, amounting to 170% when compared to the capacity of 700-W-0 at 152.17 kN. In contrast, the global control specimens averaged 161.1 kN (Fig. 23).

Similarly, using CFRP strips significantly improved the damaged specimen, reaching an ultimate flexural load of 250.2 kN (164% of control specimen 700-W-0). Hence, the use of CFRP ropes and strips is effective in recovering and improving the flexural strength of heat shock-damaged beams designed for flexure. The use of ropes gave a 4% increase in flexural capacity over strips; therefore, both materials had similar results. These findings indicate the mechanical properties of the thermally shocked beam were improved by the repair utilizing both types of NSM-CFRP. In contrast to NSM-CFRP strips, the usage of NSM-CFRP ropes is particularly effective in increasing these properties. This can be due to the NSM-CFRP ropes' effectiveness in resisting external loads beyond the point at which steel would yield, while having a greater tensile modulus than the NSM-CFRP strips. In addition, compared to CFRP strips, the rope was more effective in increasing the total energy absorbed before fracture.[34,45]

Both materials had a similar crack pattern (see Figs. 24e & k). At 120 kN for ropes and 130 kN for strips, the first cracks started to show. The load-deflection curves of the experiments (Fig. 23) show the failure mode, with 700-W-1 and 700-W-7 both beginning linearly and reaching high loads before failing suddenly and without ductility.

3.3.7 Cost-effectiveness of repair configuration

Depending on the CFRP material (rope or strip), heat shock treatment, groove placement (side or bottom), groove length, and groove profile, employing CFRP ropes and strips for repair arrangements may or may not be practical. The cost/US$ for each repaired specimen is listed in Table 9; the manufacturer provides the cost/m, and the repaired ultimate flexural capacity is determined by contrasting the repaired specimen with the control (heat-damaged) specimen. For CFRP ropes and strips, the price per meter is $17.5 USD and $39.5 USD, respectively.

As listed in Table 8, the specimens 500-W-1 and 700-W-3 had the greatest feasibility factor, 2.42 kN/US$. However, it can be concluded that (Configuration 3) utilized in 700-W-3 produced the best recovery compared to other configurations under the same heating regime by taking into account 500-W-1's usage of (Configuration 1).

The lowest recovery-to-cost ratio was observed in specimens 700-C-1 which was heated and then cooled using a CO_2 fire extinguisher. The effectiveness of repairing this specimen was hindered by the nature of the spider web thermal cracks, which were deeper and more severe compared to those in specimens cooled by water (see Fig. 16). Upon comparing 700-W-5 and 700-W-6, it is evident that 700-W-6, which utilized CFRP rope only in the high tension zone (middle of span), achieved much higher cost-effectiveness in terms of recovery; 2.03 kN/US$ compared to 1.34 kN/US$ for 700-W-5, which employed CFRP ropes for the entire span length. Considering the high cost of CFRP materials and adhesives, this approach offers opportunities to reduce the expenses

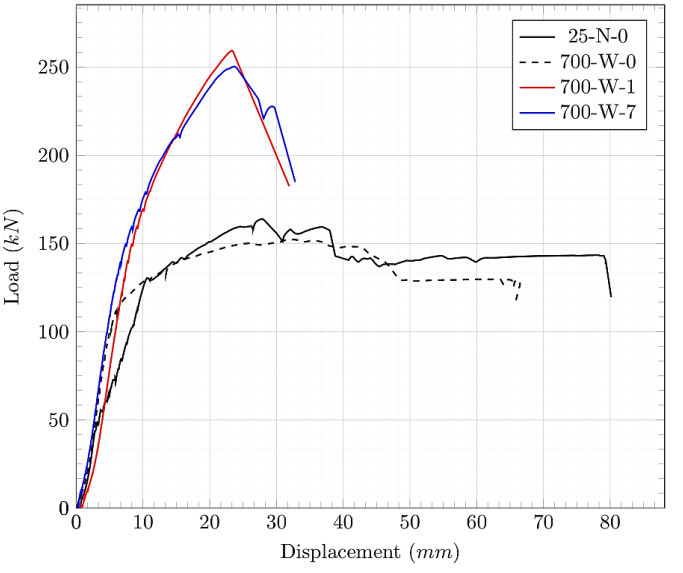

Fig. 23 Effect of CFRP material load-deflection curve.

Table 9. Cost effectiveness of FRP repairing.

Beam	Configuration	U_L	Recovered Load	FRP Repair Cost	Capacity/Cost (kN/US$)
700-W-0	Control	152.17	-	-	-
700-W-1	Configuration 1	259.34	107.2	US$ 49 (2.8 m)	2.19
700-W-2	Configuration 2	212.7	60.53	US$ 49.0 (2.80 m)	1.24
700-W-3	Configuration 3	276.65	124.5	US$ 49.0 (2.80 m)	2.42
700-W-4	Configuration 4	255.56	103.4	US$ 51.5 (2.94 m)	2.06
700-W-5	Configuration 5	283.17	131	US$ 98 (5.6 m)	1.34
700-W-6	Configuration 6	279.84	127.7	US$ 63 (3.6 m)	2.03
700-W-7	Configuration 7	250.24	98.07	US$ 110.6 (2.8 m)	0.89
700-C-0	Control	149.5	-	-	-
700-C-1	Configuration 1	172.56	23.06	US$ 49 (2.8 m)	0.47
500-W-0	Control	153.68	-	-	-
500-W-1	Configuration 1	263.64	110	US$ 49 (2.8 m)	2.24

associated with repairing damaged structures by smartly omitting unnecessary CFRP. The specific cost of the CFRP strip was 2.25 times that of CFRP rope, resulting in a much lower feasibility factor of 0.89 kN/$US for 700-W-7 (repaired using CFRP strip). However, it is important to note that although 700-W-7 was less cost-effective, the specimen did not experience FRP rupture like its counterparts repaired using CFRP ropes.

3.4 Failure modes

The failure modes for each specimen are shown in Fig. 24. Fine vertical flexural and transverse cracks were started in the midpoint of the beam, at the area of highest moment with a load of 22kN, as shown in Figs. 24a, b, c, & d. Flexural cracks widened, spread over the beam's span, and propagated all the way to the section's full depth before failing as the load increased. Both the unheated control specimens (25-N-0-1 and 25-N-0-2) and the heated control specimens (500-W-0, 700-W-0, and 700-C-0) showed a similar flexural failure mode and cracking pattern, indicating that the two heating temperatures and the cooling method had no effect on the failure mode as shown Fig. 24.

Depending on the Side NSM's repair configuration, there was a variation in the mode of failure between the Bottom and Side NSM. The failure modes for specimens 700-W-1 (Bottom NSM), 700-W-3 (Trapezoidal Side NSM), and 700-W-4 (Parabolic Side NSM) are shown in Figs. 24e, g, & h. The specimen 700-W-2 (Straight Side NSM), shown in Fig. 24f failed due to FRP debonding and concrete cover separation. The failure mode for specimens repaired using a side-and-bottom design is shown in Figs. 24i & j. The two configurations had similar cracking behavior and first cracks; 700-W-5 (full-length) experienced a combined shear failure and FRP rupture at 140 kN, while 700-W-6 (half-length) experienced a flexural-shear failure combined with FRP rupture and concrete cover separation of the bottom face at 150 kN. The failure mode for specimen 700-W-7 is shown in Fig. 24k. It was repaired utilizing a bottom configuration and NSM-CFRP strip. The shear mode of failure of the beam was abrupt. As indicated in Fig. 24a different failure mode was seen for a beam employing CO_2 as compared to water. As indicated in 500-C-1, the beams' failure mode was a combined shear failure and FRP rupture, and the failure mode was shear behavior in addition to FRP rupture.

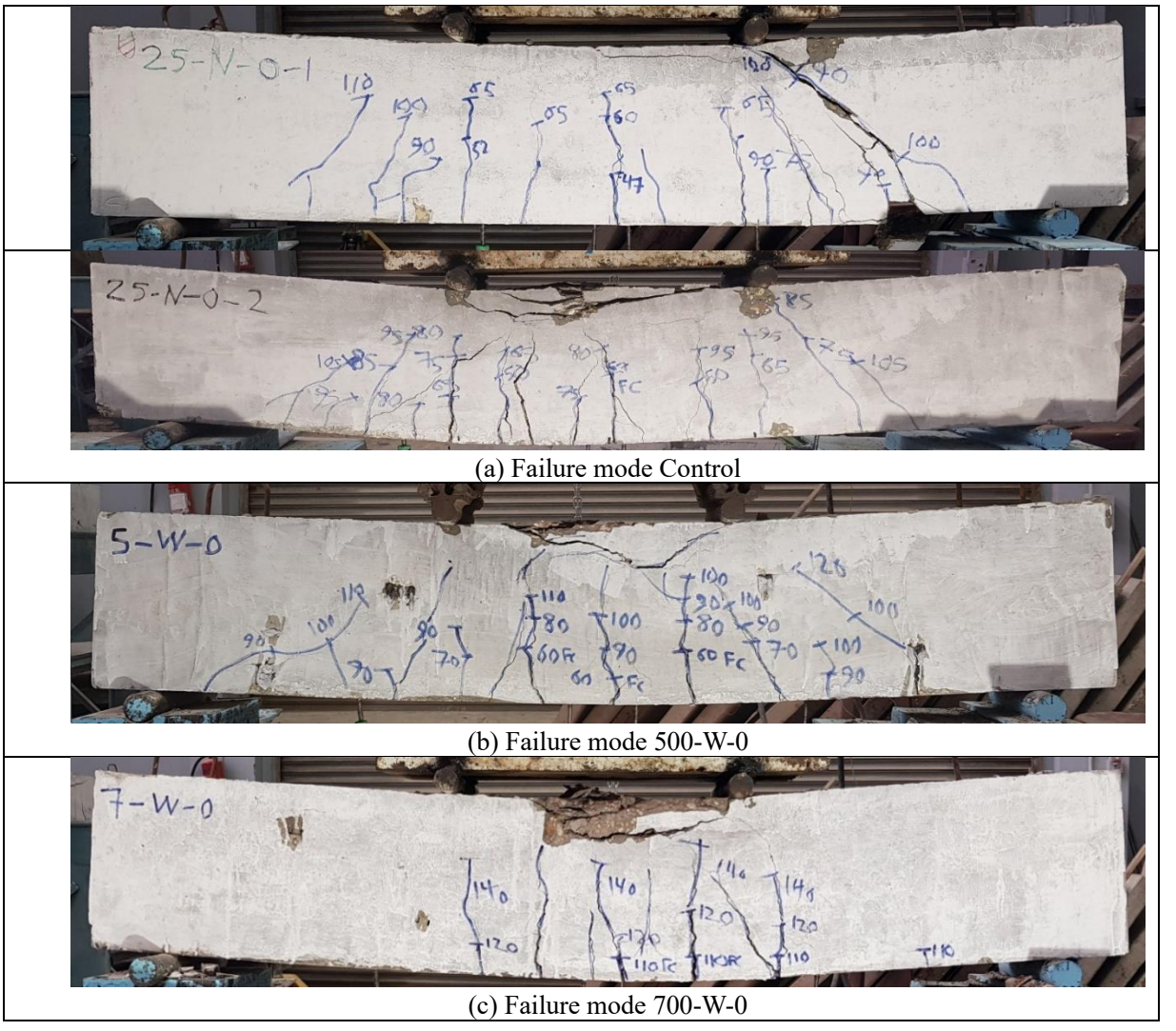

(a) Failure mode Control

(b) Failure mode 500-W-0

(c) Failure mode 700-W-0

(d)Failure mode 700-C-0

(e) FRP rope rupture 700-W-1

Failure mode 700-W-2

(g)Failure mode 700-W-3

(h)Failure mode 700-W-4

(i)Failure mode 700-W-5

(j) Failure mode 700-W-6

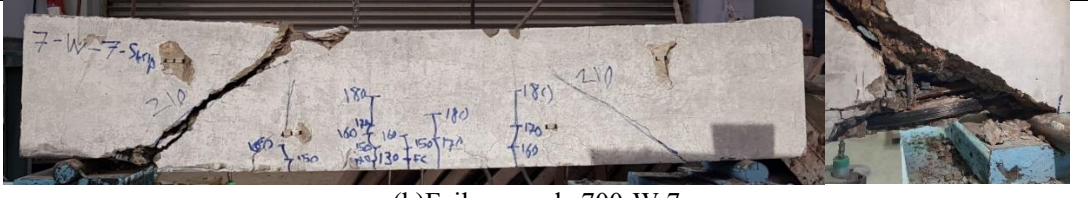

(k)Failure mode 700-W-7

Failure mode 700-C-1

Failure mode 500-C-1

Fig. 24 Failure modes of all tested specimens.

4. Conclusions

Under a Four-point flexural test, the application of CFRP ropes and strips in flexural strengthening in the tension zone was investigated. The experimental program was carried out on beam specimens that had been repaired with CFRP and had not been repaired with CFRP. The effect of the heating temperature, the cooling technique, the CFRP material, and the repair configurations were all tested. Every specimen followed the same ACI 318-11[47] and ACI 440 design specifications. seventeen beams (1400 x 250 x 150 mm) were subjected to the test. Three beams were heated to 500 °C, twelve to 700 °C, and two were designated as the global control beams. The heated beams were distributed among several cooling techniques (CO_2 fire extinguisher, water, and air). The CFRP ropes and strips were used to repair eleven heat shock-damaged specimens. In section 3, the test results were documented and evaluated to establish the efficacy of various repair configurations and the outcomes of various heating/cooling treatments.

The following conclusions from the analysis of the experimental program's data may be drawn:

1) Heat shock treatment considerably reduced HSC's compressive strength, by as much as 34% compared to the control (in the instance of concrete heated to 700 °C and cooled using CO_2 fire extinguishers). The strength loss was greater at 700 °C than at 500 °C, as was to be expected. Regarding the impact of the cooling technique, water cooling at 500 °C reduced compressive strength more than CO_2 cooling did; however, at 700 °C, water cooling reduced compressive strength somewhat less.

2) In a manner comparable, heated concrete's tensile splitting strength was significantly reduced, falling to as low as 26% of control for concrete heated to 700 °C and cooled with CO2. In terms of the impact of the cooling technique, the similar conclusion can be made: at 500 °C, water cooling resulted in lower tensile strength, but at 700 °C, CO_2 cooling resulted in lower tensile strength.

3) First cracking loads increased for all heated beam specimens, while flexure strength varied depending on the heating/cooling process. Water immersion cooling resulted in a smaller loss of flexural capacity (95% of control) than CO_2 fire extinguisher cooling, (92% of control).

4) Using CFRP significantly improved the flexural strength of repaired beams, sometimes by as much as 177% of the global control specimen (700-W-5). Furthermore, both ropes and strips worked well to recover flexural strength in the Side NSM and Bottom NSM.

5) The failure mode changed from flexural failure for the control beams to shear or combined shear and FRP rupture failure for repaired beams.

6) A more economical design by using less material directed at the high-tension zone can reduce the cost while achieving almost the same result (within 1% between 700-W-5 and 700-W-6).

7) In terms of ultimate capacity, the trapezoidal Side NSM profile exceeded the parabolic Side NSM by 8%.

Notations and Abbreviations

HSC: High Strength Concrete
NSC: Normal Strength Concrete
RC: Reinforced Concrete
SCCC: Self-Compacted Concrete
GCHA: Guinea Corn Husk Ash
FRP: Fiber Reinforced Polymers
CFRP: Carbon Fiber Reinforced Polymers
NSM: Near Surface Mounted
NSFR: Near Surface Fiber Reinforced
SNSM: Side Near Surface Mounted
UL: Ultimate Load
Us: Ultimate Displacement
YL: Yield Load
Yd: Yield Displacement
FF: Flexural Failure
SF: Shear Failure
FR: FRP Debonding

FD: Flexural Ductility
CS: Concrete Spalling
Recovered Load: The difference in ultimate load between the repaired specimen and the control specimen
FRP Repair Cost: The cost of the FRP material and adhesives used to repair the specimen
Capacity/Cost: The ratio of the recovered load to the FRP repair cost
°C: Degrees Celsius
CO_2: Carbon Dioxide
kN: Kilo Newton
mm: Millimeter
MPa: Mega Pascal
LVDTs: Linear Variable Differential Transformers
ACI: American Concrete Institute
US$: United States Dollars
W: Water cooling
C: CO_2 cooling
B: Bottom
S: Side

Conflict of Interest

There is no conflict of interest.

Supporting Information

Not applicable.

References

[1] H. S. Mahmoud, R. A. Hawileh, J. A. Abdalla, Strengthening of high strength reinforced concrete thin slabs with CFRP laminates, *Composite Structures*, 2021, **275**, 114412, doi: 10.1016/j.compstruct.2021.114412.

[2] A. S. Abdulrahman, M. R. A. Kadir, Behavior and flexural strength of fire damaged high strength reinforced rectangular concrete beams after strengthening with CFRP laminates, *Ain Shams Engineering Journal*, 2022, **13**, 101767, doi: 10.1016/j.asej.2022.101767.

[3] H. Constantinescu, O. Gherman, C. Negrutiu, S. P. Ioan, Mechanical properties of hardened high strength concrete, *Procedia Technology*, 2016, **22**, 219-226, doi: 10.1016/j.protcy.2016.01.047.

[4] L. T. Phan, L. Phan, Fire performance of high-strength concrete: a report of the state-of-the-art, National Institute of Standards and Technology Gaithersburg, MD, 1996.

[5] K. M. Anwar Hossain, High strength blended cement concrete incorporating volcanic ash: performance at high temperatures, *Cement and Concrete Composites*, 2006, **28**, 535-545, doi: 10.1016/j.cemconcomp.2006.01.013.

[6] J. H. Gamage, R. Al-Mahaidi, M. B. Wong, Durability of CFRP-strengthened concrete members under extreme temperature and humidity, *Australian Journal of Structural Engineering*, 2009, **9**, 111-118, doi: 10.1080/13287982.2009.11465014.

[7] A. M. Neville, Properties of concrete, Longman London, 1995.

[8] Q. Ma, R. Guo, Z. Zhao, Z. Lin, K. He, Mechanical properties of concrete at high temperature—a review, *Construction and Building Materials*, 2015, **93**, 371-383, doi: 10.1016/j.conbuildmat.2015.05.131.

[9] Y. Al Rjoub, M. Tamimi, Heat transfer and thermal shock of recycled glass concrete, *Magazine of Civil Engineering*, 2019, 27-38, doi: 10.18720/MCE.91.3.

[10] I. A. Sharaky, S. S. Ahmad, A. M. El-Azab, H. S. Khalil, Strength and mass loss evaluation of HSC with silica fume and nano-silica exposed to elevated temperatures, *Arabian Journal for Science and Engineering*, 2022, **47**, 4187-4209, doi: 10.1007/s13369-021-06006-7.

[11] E. F. T. Carvalho, J. T. D. Silva Neto, P. R. R. Soares Junior, P. S. Maciel, H. L. Fransozo, A. C. D. S. Bezerra, A. M. C. Gouveia, Influence of cooling methods on the residual mechanical behavior of fire-exposed concrete: an experimental study, *Materials*, 2019, **12**, 3512, doi: 10.3390/ma12213512.

[12] W. Botte, R. Caspeele, Post-cooling properties of concrete exposed to fire, *Fire Safety Journal*, 2017, **92**, 142-150, doi: 10.1016/j.firesaf.2017.06.010.

[13] A. F. Bingöl, R. Gül, Effect of elevated temperatures and cooling regimes on normal strength concrete, *Fire and Materials*, 2009, **33**, 79-88, doi: 10.1002/fam.987.

[14] R. Z. Al-Rousan, R. H. Haddad, A. O. Swesi, Repair of shear-deficient normal weight concrete beams damaged by thermal shock using advanced composite materials, *Composites Part B: Engineering*, 2015, **70**, 20-34, doi: 10.1016/j.compositesb.2014.10.032.

[15] S. O. Odeyemi, M. A. Anifowose, R. Abdulwahab, W. O. Oduoye, Mechanical properties of high-performance concrete with Guinea corn husk ash as additive, *LAUTECH Journal of Civil and Environmental Studies*, 2020, **5**, 131-145, doi: 10.36108/laujoces/0202/50(0131).

[16] F. Ali, Is high strength concrete more susceptible to explosive spalling than normal strength concrete in fire? *Fire and Materials*, 2002, **26**, 127-130, doi: 10.1002/fam.791.

[17] E. G. Choi, Y. S. Shin, The structural behavior and simplified thermal analysis of normal-strength and high-strength concrete beams under fire, *Engineering Structures*, 2011, **33**, 1123-1132, doi: 10.1016/j.engstruct.2010.12.030.

[18] V. K. R. Kodur, F.-P. Cheng, T.-C. Wang, M. A. Sultan, Effect of strength and fiber reinforcement on fire resistance of high-strength concrete columns, *Journal of Structural Engineering*, 2003, **129**, 253-259, doi: 10.1061/(asce)0733-9445(2003)129:2(253).

[19] V. Kodur, R. McGrath, Fire endurance of high strength concrete columns, *Fire Technology*, 2003, **39**, 73-87, doi: 10.1023/A: 1021731327822.

[20] V. K. R. Kodur, L. Phan, Critical factors governing the fire performance of high strength concrete systems, *Fire Safety Journal*, 2007, **42**, 482-488, doi: 10.1016/j.firesaf.2006.10.006.

[21] Y. H. Mugahed Amran, R. Alyousef, R. S. M. Rashid, H. Alabduljabbar, C.-C. Hung, Properties and applications of FRP in strengthening RC structures: a review, *Structures*, 2018, **16**, 208-238, doi: 10.1016/j.istruc.2018.09.008.

[22] A. Landesmann, C. A. Seruti, E. de Miranda Batista, Mechanical properties of glass fiber reinforced polymers members for structural applications, *Materials Research*, 2015, **18**, 1372-1383, doi: 10.1590/1516-1439.044615.
[23] P. K. Mallick, Fiber-Reinforced Composites: Materials, Manufacturing, and Design, Third Edition, CRC Press, 2007, doi: 10.1201/9781420005981.
[24] D. Matykiewicz, Biochar as an effective filler of carbon fiber reinforced bio-epoxy composites, *Processes*, 2020, **8**, 724, doi: 10.3390/pr8060724.
[25] Y. Al Rjoub, A. Obaidat, A. Ashteyat, K. Alshboul, Experimental and analytical investigation of using externally bonded, hybrid, fiber-reinforced polymers to repair and strengthen heated, damaged RC beams in flexure, *Journal of Structural Fire Engineering*, 2022, **13**, 391-417, doi: 10.1108/jsfe-09-2021-0059.
[26] A. M. Ashteyat, A. T. Obaidat, Y. T. Obaidat, M. Abdel-Jaber, D. Al-Tarawneh, The behavior of strengthened and repaired RC columns with (CFRP) rope under different preloading levels, *European Journal of Environmental and Civil Engineering*, 2023, **27**, 4212-4236, doi: 10.1080/19648189.2023.2179668.
[27] A. T. Obaidat, Compression behavior of confined circular reinforced concrete with spiral CFRP rope with different slenderness ratios, *Results in Engineering*, 2022, **16**, 100615, doi: 10.1016/j.rineng.2022.100615.
[28] A. T. Obaidat, Y. T. Obaidat, Behavior of repaired projectile bullet damaged reinforced concrete beams using CFRP sheet in conjunction with natural aggregate or recycled aggregate concrete layer, *European Journal of Environmental and Civil Engineering*, 2023, **27**, 3473-3488, doi: 10.1080/19648189.2022.2140205.
[29] A. T. Obaidat, A. M. Ashteyat, Y. T. Obaidat, A. Y. Al-Btoush, S. Hanandeh, Experimental and numerical study of strengthening and repairing heat-damaged RC circular column using hybrid system of CFRP, *Case Studies in Construction Materials*, 2021, **15**, e00742, doi: 10.1016/j.cscm.2021.e00742.
[30] Y. T. Obaidat, A. M. Ashteyat, A. Taleb Obaidat, M. N. Abu-Lebdeh, Bond characteristics between concrete and near-surface mounted carbon fiber reinforced polymer cords, *Journal of Structural Integrity and Maintenance*, 2021, **6**, 223-236, doi: 10.1080/24705314.2021.1950379.
[31] Y. T. Obaidat, W. S. Barham, B. N. Abdelrahman, Effect of elevated temperature on the bond behavior between near Surface Mounted-Carbon Fiber Reinforced Polymers strips and Recycled Aggregate concrete, *Construction and Building Materials*, 2020, **251**, 118970, doi: 10.1016/j.conbuildmat.2020.118970.
[32] Y. T. Obaidat, W. S. Barham, A. T. Obaidat, K. M. Attar, Behavior of NSM CFRP reinforced concrete columns: experimental and analytical work, *Case Studies in Construction Materials*, 2021, **15**, e00589, doi: 10.1016/j.cscm.2021.e00589.
[33] Y. T. Obaidat, A. T. Obaidat, A. M. Ashteyat, Behaviour of heat damaged repaired reinforced SCC cantilever beam using carbon fiber reinforced polymer rope, *European Journal of Environmental and Civil Engineering*, 2022, **26**, 8002-8017, doi: 10.1080/19648189.2021.2016496.
[34] A. T. Obaidat, Flexural behavior of reinforced concrete beam using CFRP hybrid system, *European Journal of Environmental and Civil Engineering*, 2022, **26**, 6165-6187, doi: 10.1080/19648189.2021.1934552.
[35] R. Parretti, A. Nanni, Strengthening of RC members using near-surface mounted FRP composites: design overview, *Advances in Structural Engineering*, 2004, **7**, 469-483, doi: 10.1260/1369433042863198.
[36] M. Al-Zu'bi, M. Fan, Y. Al Rjoub, A. Ashteyat, M. J. Al-Kheetan, L. Anguilano, The effect of length and inclination of carbon fiber reinforced polymer laminates on shear capacity of near-surface mounted retrofitted reinforced concrete beams, *Structural Concrete*, 2021, **22**, 3677-3691, doi: 10.1002/suco.202100198.
[37] S. Ahmed, I. A. Sharaky, Y. E. Ibrahim, A. Abdo, Flexural response of gfrp rc beams strengthened with side and bottom nsm gfrp bars, *Case Studies in Construction Materials*, 2023, **18**, e01858, doi: 10.1016/j.cscm.2023.e01858.
[38] F. A. Megahed, M. H. Seleem, A. A. M. Badawy, I. A. Sharaky, The flexural response of RC beams strengthened by EB/NSM techniques using FRP and metal materials: a state-of-the-art review, *Innovative Infrastructure Solutions*, 2023, **8**, 289, doi: 10.1007/s41062-023-01245-z.
[39] Z. K. Szabó, G. L. Balázs, Near surface mounted FRP reinforcement for strengthening of concrete structures, *Periodica Polytechnica Civil Engineering*, 2007, **51**, 33, doi: 10.3311/pp.ci.2007-1.05.
[40] Y. T. Obaidat, A. M. Ashteyat, A. T. Obaidat, S. F. Alfaris, A new technique for repairing reinforced concrete columns, *Journal of Building Engineering*, 2020, **30**, 101256, doi: 10.1016/j.jobe.2020.101256.
[41] Y. S. Al Rjoub, A. M. Ashteyat, Y. T. Obaidat, S. Bani-Youniss, Shear strengthening of RC beams using near-surface mounted carbon fibre-reinforced polymers, *Australian Journal of Structural Engineering*, 2019, **20**, 54-62, doi: 10.1080/13287982.2019.1565617.
[42] A. T. Obaidat, A. M. Ashteyat, S. Hanandeh, A. Y. Al-Btoush, Behavior of heat damaged circular reinforced concrete columns repaired using Carbon Fiber Reinforced Polymer rope, *Journal of Building Engineering*, 2020, **31**, 101424, doi: 10.1016/j.jobe.2020.101424.
[43] I. A. Sharaky, L. Torres, J. Comas, C. Barris, Flexural response of reinforced concrete (RC) beams strengthened with near surface mounted (NSM) fibre reinforced polymer (FRP) bars, *Composite Structures*, 2014, **109**, 8-22, doi: 10.1016/j.compstruct.2013.10.051.
[44] I. A. Sharaky, R. M. Reda, M. Ghanem, M. H. Seleem, H. E. M. Sallam, Experimental and numerical study of RC beams strengthened with bottom and side NSM GFRP bars having different end conditions, *Construction and Building Materials*, 2017, **149**, 882-903, doi: 10.1016/j.conbuildmat.2017.05.192.
[45] R. H. Haddad, A. N. Harb, CFRP ropes for retrofitting heat-damaged concrete beams, *Journal of Building Engineering*, 2021, **43**, 102522, doi: 10.1016/j.jobe.2021.102522.

[46] A. M. Ashteyat, R. Haddad, Y. T. Obaidat, Repair of heat-damaged SCC cantilever beams using SNSM CFRP strips, *Structures*, 2020, **24**, 151-162, doi: 10.1016/j.istruc.2020.01.005.
[47] A. A. Standard, Building code requirements for structural concrete (ACI 318-11), *American Concrete Institute*, 2011.
[48] H.-J. Chen, C.-C. Chen, H.-S. Lin, S.-K. Lin, C.-W. Tang, Flexural behavior of ultra-high-performance fiber-reinforced concrete beams after exposure to high temperatures, *Materials*, 2021, **14**, 5400, doi: 10.3390/ma14185400.
[49] Y. N. Chan, X. Luo, W. Sun, Compressive strength and pore structure of high-performance concrete after exposure to high temperature up to 800°C, *Cement and Concrete Research*, 2000, **30**, 247-251, doi: 10.1016/S0008-8846(99)00240-9.

